

Amorphous 1-propanol interstellar ice beyond its melting point

R. Ramachandran¹,¹★† A. Hazarika²,²† S. Gupta,¹ S. Nag²,² J. K. Meka,¹ Tejender S. Thakur³,³ S. Yashonath,⁴ G. Vishwakarma,⁵ S.-L. Chou⁶,⁶ Y.-J. Wu,⁶ P. Janardhan,¹ B. N. Rajasekhar,⁷ Anil Bhardwaj,¹ N. J. Mason,⁸ B. Sivaraman¹★ and Prabal K. Maiti²★

¹Physical Research Laboratory, Ahmedabad 380009, India

²Center for Condensed Matter Theory, Department of Physics, Indian Institute of Science, Bangalore 560012, India

³Biochemistry and Structural Biology Division, CSIR–Central Research Drug Institute, Lucknow 226301, India

⁴Solid State and Structural Chemistry Unit, Indian Institute of Science, Bangalore 560012, India

⁵DST Unit of Nanoscience (DST UNS) and Thematic Unit of Excellence (TUE), Department of Chemistry, Indian Institute of Technology Madras, Chennai 600036, India

⁶National Synchrotron Radiation Research Center, Hsinchu 300092, Taiwan

⁷Atomic and Molecular Physics Division, Bhabha Atomic Research Centre, Mumbai 400085, India

⁸School of Physical Sciences, University of Kent, Canterbury CT2 7NH, UK

Accepted 2024 February 14. Received 2024 February 5; in original form 2023 November 23

ABSTRACT

The recent discovery of 1-propanol (CH₃CH₂CH₂OH) in the interstellar medium (ISM) is of tremendous interest since fatty alcohols have been proposed as constituents of proto-cell membranes. Motivated by this discovery, we present the laboratory mid-infrared (MIR) and vacuum ultraviolet (VUV) absorption spectra of 1-propanol ice under astrochemical conditions, mimicking an icy mantle on cold dust in the ISM. Both MIR and VUV spectra were recorded at ultrahigh vacuum of $\sim 10^{-9}$ mbar and at temperatures ranging from 10 K to sublimation. The morphology of the 1-propanol ice deposited at 10 K was amorphous. By warming the ice to temperatures of 140 K and above, with subsequent recording of IR spectra, we observe complete sublimation of 1-propanol molecules from the substrate around 170 K. No amorphous-to-crystalline phase change was observed upon warming to higher temperatures. Additionally, we observe the IR and VUV signatures of 1-propanol ice on the substrate well beyond its melting point (147 K). To the best of our knowledge, this is the first reported observation of a molecular ice staying well beyond its melting point under such conditions. This result shows that the morphology of icy mantles on ISM cold dust grains is more complex than previously thought. Our atomistic molecular dynamics simulations capture the experimental trends and shed light on the microscopic origin of this unusual phase behaviour of 1-propanol.

Key words: astrochemistry – molecular data – methods: statistical – software: simulations – ISM: molecules – infrared: general.

1 INTRODUCTION

Since the identification of methanol and ethanol (Ball et al. 1970; Zuckerman et al. 1975), it has become well-established that molecules containing the hydroxyl (OH) group are present in the interstellar medium (ISM; e.g. Turner & Apponi 2001; Hollis et al. 2004). These molecules are also known to be the constituents of the icy surfaces found within the Solar system (e.g. Despois 1992; Crovisier et al. 2004). In fact, their role in the chemistry of complex molecular evolution is quite central as they hold large amounts of hydrogen within their structure. The physicochemical nature of methanol and ethanol in the ISM is quite well explored (Ehrenfreund & Charnley 2000). The formation of these simple alcohols is known to occur through the irradiation of mixtures of simpler molecules

such as carbon monoxide, ammonia, and water (Kasamatsu et al. 1997; Watanabe & Kouchi 2002; Hiraoka, Mochizuki & Wada 2006). Additionally, a pathway via hydrogenation of formaldehyde is also known to synthesize methanol (Fuchs et al. 2009).

With the discovery of simple alcohols, the search for larger alcohols has intensified. The detection of propanol in the ISM (Hollis et al. 2004) provided evidence of the possible presence of fatty alcohols in the ISM, as aldehydes can be considered proxy molecules for their corresponding alcohols. This was further supported by the identification of propanol in the comet CG-67P (Altwegg et al. 2017). Laboratory experiments have also demonstrated that propanol can be synthesized alongside simple alcohols by irradiating a mixture of carbon monoxide and methane with energetic electrons (Abplanalp & Kaiser 2019). A hydrogenation pathway from carbon monoxide during its freeze-out phase, in the presence of acetylene, is also known to synthesize 1-propanol (Altwegg et al. 2017).

Given that propanol can be synthesized through multiple pathways under the cold dust conditions of the ISM, its presence in the ISM was anticipated to be within detectable limits. As expected, focused

* E-mail: ragav.kasak@gmail.com (RR); bhala@prl.res.in (BS); maiti@iisc.ac.in (PKM)

† Co-first authors.

observations confirmed the presence of 1-propanol in the ISM (Jiménez-Serra et al. 2022). This discovery is of tremendous interest since fatty alcohols have been proposed as constituents of protocell membranes (Ruiz-Mirazo, Briones & de la Escosura 2014). However, our understanding of the physicochemical nature of 1-propanol in the ISM remains quite limited. Although reports exist on the infrared (IR) spectra of this molecule in both liquid and ice phases (Doroshenko, Pogorelov & Sablinskas 2012; Hudson & Moore 2018; Qasim et al. 2019), detailed experiments on the temperature-dependent behaviour of 1-propanol ice are scarce. Therefore, we conducted an experimental investigation of this fatty alcohol under astrochemical icy conditions.

To support and interpret the experimental findings, we also employed molecular dynamics (MD) simulations for the 1-propanol system. While computer simulations have been extensively used to investigate this molecule in its liquid and gas phases (Zangi 2018; Pethes et al. 2021), research into its ice phase remains scarce. Previously, we have studied the ice phase of another astrochemical complex organic molecule (COM) methanol using MD simulation (Nag et al. 2023) and explained the recent experimental observation of the same molecule (Luna et al. 2018). By employing computational techniques, we aim not only to reproduce and elucidate the experimental results but also to delineate the physicochemical properties of 1-propanol. A comprehensive understanding of 1-propanol, achieved through a combination of experimental and computational approaches, is crucial in astrochemistry due to its relevance as a precursor to more COMs and its potential role as an indicator of life's fundamental components (Ruiz-Mirazo et al. 2014). This study will not only enhance our fundamental knowledge of this molecule but also shape the trajectory of future studies of similar organic molecules.

2 METHODOLOGY

Three different techniques were employed to investigate the 1-propanol ice under astrochemical conditions. The details of each technique are elaborated below. For all the experiments 1-propanol in liquid form, procured from Merck (purity ≥ 99.9 per cent), was used.

2.1 Vacuum ultraviolet spectroscopy

Vacuum ultraviolet (VUV) experiments of 1-propanol ices were conducted using VUV light from beamline BL-03 of the Taiwan Light Source (TLS) at the National Synchrotron Radiation Research Centre (NSRRC), Taiwan. One of the end stations of the beamline is connected to an ultrahigh vacuum (UHV) chamber containing a closed cycle helium cryostat with a VUV transparent lithium-fluoride (LiF) window attached to its cold finger using a copper substrate holder. This window is cooled down to 10 K and serves as the interstellar dust analogue. Detailed discussions of the experimental set-up, liquid sample preparation, and the spectral acquisition have been presented in Lu et al. (2008), and the chamber set-up is similar to one shown in fig. 2 of Ramachandran et al. (2023).

A VUV spectrum, spanning 115–220 nm with a step size of 1 nm, of the blank LiF window at 10 K was recorded at the beginning of each experiment. This spectrum was used as I_0 for the respective experiments. The sample was then deposited on the LiF window using a deposition technique similar to that explained in the previous section. Spectra recorded after deposition are used as I . From I_0 and I , the VUV spectra of 1-propanol ice were calculated using the Beer–Lambert law. After deposition and obtaining a spectrum at 10 K, the

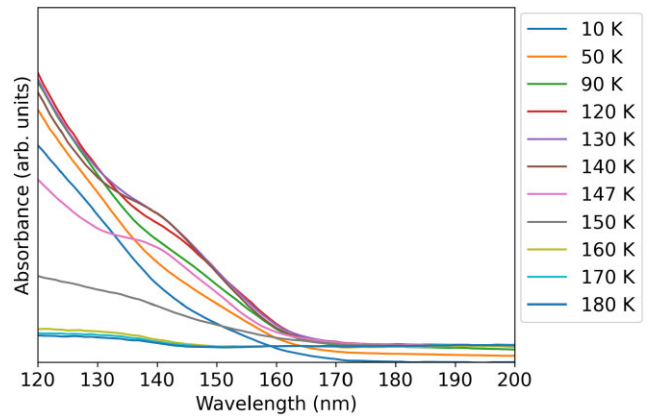


Figure 1. VUV spectra of 1-propanol ice recorded after deposition at 10 K. The deposited ice was then warmed to higher temperatures and spectra recorded at specific temperatures until sublimation.

ice was heated to higher temperatures until sublimation, with VUV spectra recorded at regular intervals.

2.2 Mid-infrared spectroscopy

The astrochemical icy mantle conditions were recreated using the Simulator for Astromolecules at Low Temperature (SALT) facility housed at the Physical Research Laboratory, Ahmedabad. The experimental system can achieve pressures of 10^{-10} mbar at 10 K. A zinc-selenide (ZnSe) substrate is used as the ISM dust analogue, which, when placed on the substrate holder at the tip of the closed-cycle helium cryostat, reaches temperatures as low as 10 K while the system is under UHV conditions. A cryogenic temperature controller (Lakeshore) regulates the sample's temperature and heating rate. A detailed description of this set-up can be found in Ramachandran et al. (2023). In these experiments, a heating rate of 5 K min^{-1} was primarily employed. The deposited molecular ices were probed *in situ* using IR spectroscopy (Nicolet iS 50 FTIR Spectrometer), in the mid-IR (MIR) range (4000 to 650 cm^{-1} ; resolution 4 cm^{-1} and integration time 86 s).

1-propanol from the sample holder was vapour deposited (through a differential pressure technique) on to the ZnSe window maintained at 10 K. Deposition was carried out for approximately 50 s at a pressure of around 7×10^{-9} mbar. A post-deposition IR spectrum was recorded at 10 K. The resultant ice was then heated at the rate of 5 K min^{-1} in 10 K increments until 140 K, with subsequent recording of IR spectra. After 140 K, the sample was heated to 145, 146, 147, and 150 K, with IR spectra recorded for each temperature. Beyond 150 K the sample was heated in 5 K increments, and IR spectra were recorded until sublimation. Deposition was also performed at 130, 145, 150, 160, 170, 180, and 185 K. In all these cases, the ice was heated at the rate of 5 K min^{-1} until sublimation, with subsequent recording of IR spectra.

2.3 Computational details

In order to obtain a better understanding of the phase behaviour of 1-propanol, a vacuum-deposited film of 1-propanol on potassium-bromide (KBr) surface was simulated, and subsequently, the density of states (DoS) spectra was calculated in simulation as a function of temperature. To model 1-propanol, the all-atom OPLS-AA (Jorgensen & Tirado-Rives 2005; Dodda et al. 2017b) force-field parameters were used. The LigParGen (Dodda et al. 2017a)

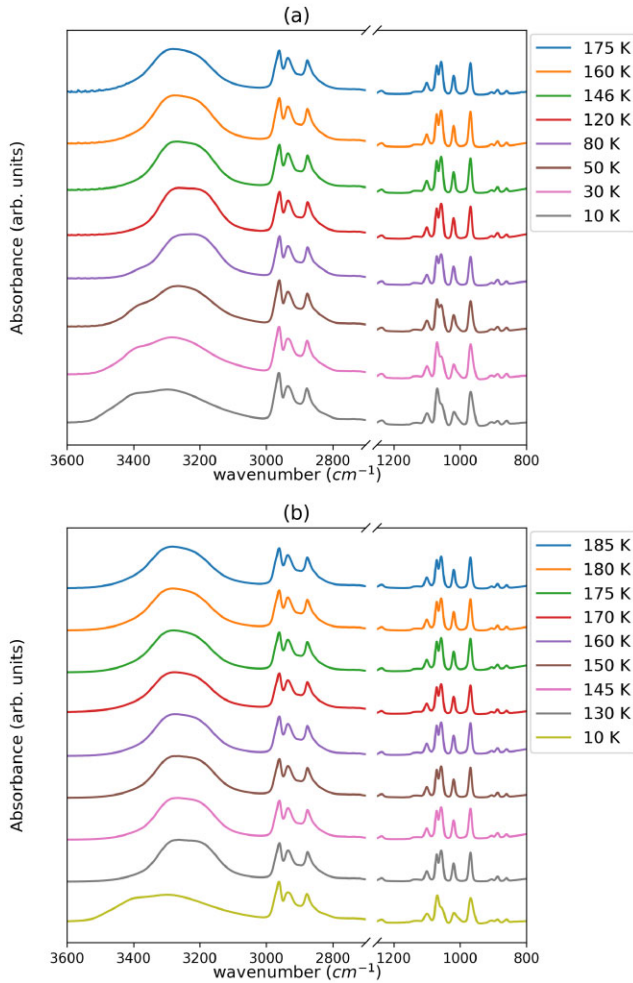


Figure 2. (a) MIR spectra of 1-propanol ice recorded after deposition at 10 K. The ice was then warmed to higher temperatures with subsequent recording of spectra at specific temperatures until sublimation. A spectrum around the melting point of 1-propanol (~ 147 K) was recorded. Beyond the melting point a significant amount of 1-propanol was observed to be present until sublimation around 175 K. (b) MIR spectra of 1-propanol ice deposited at 10 K and higher temperatures ranging from 130 to 185 K, respectively. These correspond to temperatures a few K above and below the melting point of 1-propanol. Molecules of 1-propanol are found to adhere and form layers on the dust analogues even beyond its melting point.

topology generator for the aforementioned force field was utilized to generate the topology in GROMACS-compatible format, which was subsequently used for all MD simulations. Further, to take into account the Coulombic interactions, electrostatic potential (ESP) charges were used as atomic partial charges. These charges were obtained during crystal structure prediction (CSP) calculation. All the force field parameters are tabulated in Tables S1–S5 in the Supporting Information (SI). For modelling of KBr, the potential parameters developed by Barbosa (Fuentes-Azcatl & Barbosa 2018) were used. The same potential parameters for KBr had been used in our earlier work on methanol adsorbed to KBr substrate (Nag et al. 2023). Lorentz–Berthelot mixing rules were applied for non-bonded interactions between 1-propanol and KBr.

For benchmarking the applicability of OPLS-FF parameters, several thermodynamic and spectroscopic properties of 1-propanol in liquid and gas phases such as bulk density, specific heat, and vibrational spectra under atmospheric pressure were obtained in

simulation and compared with known values of these properties (Stromsoe, Ronne & Lydersen 1970; NIST 2023). The methodology is described and the benchmarking results are tabulated in the SI. Using OPLS-FF as the forcefield (FF) of choice, a very good agreement could be seen between simulation and experiment (see Table S6 in SI).

After benchmarking the FF against 1-propanol, the molecule of interest, the simulated deposition of 1-propanol was performed using the PYTHON package PYTHINFILM (Stroet et al. 2022). PYTHINFILM, or PYTF, acts as a PYTHON-based frontend to run classical MD deposition simulations using GROMACS (Abraham et al. 2015) as the MD engine. The deposition was carried out using the ‘vacuum deposition’ method which can be described as the insertion of the molecule at a distance (hence called insertion distance) away from the substrate, and letting the dynamics run until the molecule settles on the substrate; the entire system is kept under a tall column of vacuum during this entire step. This step in the process is carried out one by one on a per-molecule basis until the desired number of molecules have been successfully deposited on the surface. For our system, the insertion distance was set to 8 nm, while the column of the vacuum was chosen to be 20 nm long. All the details of the deposition simulations are provided in the SI.

All the MD simulations were performed using the GROMACS 2023.1 (Abraham et al. 2015) MD package. The deposited system of 1-propanol in vacuum on the KBr substrate was simulated in the constant temperature (NVT) ensemble using the stochastic velocity rescaling thermostat (Bussi, Donadio & Parrinello 2007) with temperature coupling constant value fixed at 1 ps. A 1 fs integration time-step was employed to simulate the system with an updated neighbour list every 100 time-steps. For short-range LJ and electrostatic interaction, the cut-off distance was set to 12 Å. Long-range electrostatics were handled via the particle mesh ewald (PME; Darden, York & Pedersen 1993) method using fourth-order interpolation (Essmann et al. 1995) while the Fourier spacing was kept at 0.16 nm.

At all temperatures, the equilibration runs were carried out for at least 20 ns and extended further depending on the convergence of potential energy to ensure thorough thermalization. This was followed by a 30 ps simulation in the NVT ensemble to compute the corresponding density of states using the 2PT algorithm (Lin, Blanco & Goddard 2003; Lin, Maiti & Goddard 2010). During the 30 ps NVT simulation run to obtain DoS, the coordinates, velocities, and energies were stored at every 2 fs.

3 RESULTS AND DISCUSSION

3.1 Experimental results (VUV and IR)

VUV spectra of 1-propanol ice, deposited at 10 K and subsequently warmed to higher temperatures, are shown in Fig. 1 for selected temperatures. At 10 K, the ice exhibits a broad absorption, with no fine structures visible between 115 and 170 nm. As the ice is warmed to higher temperatures, the spectra reveal a peak around 142 nm at 120 K, which intensifies upon further warming to 130 and 140 K. The spectrum recorded upon warming the ice to 147 K (melting point of 1-propanol ice at atmospheric pressure; Tschamler, Richter & Wettig 1949) remains similar to the spectrum at 140 K, with a slight reduction in absorbance intensity. We compare the melting point at atmospheric pressure with the ice characteristics at UHV because even though melting points at UHV are unavailable in literature for most molecules, it can be conjectured that they will be lower than the melting point at atmospheric pressure. Hence, in this paper, melting

point implies melting point at atmospheric pressure. The heating was continued to temperatures as high as 170 K, revealing weak absorbance in the lower wavelength range of 115–145 nm.

A similar experiment employing IR spectral probing was conducted on 1-propanol ice. The resulting spectra at a few selected temperatures are presented in Fig. 2. The spectrum of the 1-propanol ice at 10 K exhibited all the expected peaks, such as those corresponding to OH symmetric stretching, CH₃ and CH₂ symmetric stretching, and CH₂ asymmetric stretching, CH₃ rocking and CH₂-O stretching vibrations. The ice was then warmed to higher temperatures, up to 175 K, with subsequent recording of spectra.

Upon close examination of the spectral signatures, we focus on the OH symmetric stretching and CH₃ rocking vibrations. As evident from Fig. 2 (a), significant changes are observed in these two peaks as the ice is warmed from 10 to 175 K. The peak corresponding to the OH stretching vibration at 10 K was much broader and featured a shoulder peak. As the ice was warmed, the shoulder peak gradually disappeared, and the OH stretching vibration appeared as a single peak, significantly narrower than the peak observed at 10 K. However, the width of the OH stretching vibration was observed to widen slightly as the ice was further warmed to 160 K. At 175 K, the peak intensity had reduced, but the peak position and width remained similar to the spectrum at 160 K.

The band at 1069 cm⁻¹ assigned to the CH₃ rocking vibration had a shoulder peak, around 1058 cm⁻¹, at 10 K, which was observed to intensify. Notably, in the spectrum recorded at 50 K, the intensity increase was significant. The intensities of these two peaks were nearly equal in the spectrum recorded at 80 K. However, the intensity of the 1058 cm⁻¹ peak continued to increase, as observed in the spectra recorded at higher temperatures, from 120 to 160 K. At 175 K, despite a significant reduction in absorbance, the intensity of the 1058 cm⁻¹ peak remained well above that of the 1069 cm⁻¹ peak. No significant changes were observed in the remaining peaks in the MIR spectra of 1-propanol ice from 10 to 175 K.

While VUV spectra revealed the presence of 1-propanol ice well beyond the melting point of the ice, the only observable change was the broad spectral signature with a slight intensity variation at 140 K. However, in the IR spectral probing of 1-propanol ice, significant changes were observed in the OH stretching and CH₃ rocking vibrations, indicative of molecular reorientation occurring as the amorphous ice formed at 10 K was warmed to higher temperatures. The reduction in the breadth of the OH band is attributed to ice compaction. The intensity reversal observed between the 1071 and 1057 cm⁻¹ band is also indicative of ice compaction as the ice tended towards a more ordered structure. Notably, the signatures for crystalline 1-propanol ice were entirely absent in the IR spectra, as no sharpening or splitting of the bands was observed.

The deposition was also performed at 130, 145, 150, 160, 170, 180, and 185 K, with the corresponding IR spectra shown in Fig. 2 (b). In each case, the ice was warmed until sublimation, and IR signatures of the ice were observed up to 185 K. However, at 180 and 185 K, the ice could only remain on the substrate for approximately 1 min. The deposited ice was amorphous and maintained its amorphous state throughout the experiments.

It is noteworthy that we were able to record the VUV and IR spectrum of 1-propanol well beyond its melting point (147 K), and the ice was observed to remain amorphous throughout the warming process, from 10 to 175 K, until sublimation. This marks the first observation of a molecule staying on a cold substrate well beyond its melting point in a UHV chamber. It is also worth mentioning that 2-propanol, a positional isomer of 1-propanol, does not show such a behaviour. It does crystallize (120 K), and sublimates (150 - 155 K)

before melting point (184 K; Ayling et al. 2017). In Table S8 in the SI, we compare the melting point and sublimation temperatures under UHV conditions for molecular ices formed on cold substrates, analogous to astrochemical icy conditions. The comparison is made between samples that exist as liquids at the standard temperature and pressure (STP) condition and ices formed by extracting vapours from their liquid counterparts. To date, the molecular ices are known to either sublime or exhibit reversible phase change as they approach the melting point (Pavithraa et al. 2017). However, from the spectral signatures, it is clearly evident that 1-propanol is present well beyond its known melting point, even under UHV conditions. We suspect the low vapour pressure of 1-propanol at such low temperatures could be the reason for the presence of this molecule well beyond the melting point. This conclusion is supported by a series of experiments where 1-propanol ice was warmed from 10 K to higher temperatures, such as 150, 160, and 170 K. Rate of loss of 1-propanol molecules from the substrate under isothermal conditions was observed to follow the following order: 170 K > 160 K > 150 K.

3.2 Computational results

3.2.1 Predicted crystal structure of 1-propanol

Under astrochemical icy conditions, most of the molecular ices, especially lighter molecules, are known to exhibit the amorphous-to-crystalline phase transition (e.g. Yuan, Smith & Kay 2016; Pavithraa et al. 2017, and many others) which naturally raises the question of its possibility for 1-propanol under similar conditions. As the crystal structure of 1-propanol is not yet experimentally known, the technique of CSP to obtain the possible crystal structure of this molecule is key to investigating this phenomenon. In the context of comparing and understanding the possibility of phase transition between crystalline and amorphous phases, knowing the predicted crystal structure provides valuable insights. It serves as a reference point for understanding the differences between the two phases, from a structural and molecular point of view. Through comparisons between the crystal structure and the amorphous state of the deposited layer, one can pinpoint differences in molecular arrangement, bonding, or other structural aspects, shedding light on the factors responsible for the phase behaviour of the molecule under astrochemical conditions.

To obtain the initial crystal structure of 1-propanol, theoretical CSP calculations were run. The top 100 ranked structures obtained from the forcefield-based rigid CSP computations for 1-propanol were initially saved as candidates. The crystal structure search was performed using the electrostatic potential derived (ESPD) atomic charges considering $Z' = 1$ in the top 22 space groups covering 95 per cent of total occurrences in the Cambridge structural data base. Input geometry and ESPD charges used in the CSP computation were obtained from gas phase DFT computations performed using meta-GGA M06-2X functional with 6-311++G(d,p) basis. From the 100 structures, the final choice was selected to be the best guess, as the unit cell was isostructural with *n*-pentanol (Ramírez-Cardona et al. 2005), another primary alcohol. Section S4 of SI contains the comprehensive procedure for predicting the crystal structure of 1-propanol using CSP.

The chosen crystal structure is a monoclinic unit cell as shown in Fig. 3. The unit cell lengths are ($a = 4.4354 \text{ \AA}$, $b = 4.4702 \text{ \AA}$, $c = 19.7348 \text{ \AA}$), and the angles ($\alpha = \gamma = 90^\circ$, $\beta = 95.1940^\circ$). To confirm the low-temperature stability of this crystal structure, a steepest descent energy minimization followed by an NPT simulation at 10 K, and atmospheric pressure was carried out for 10 ns with a

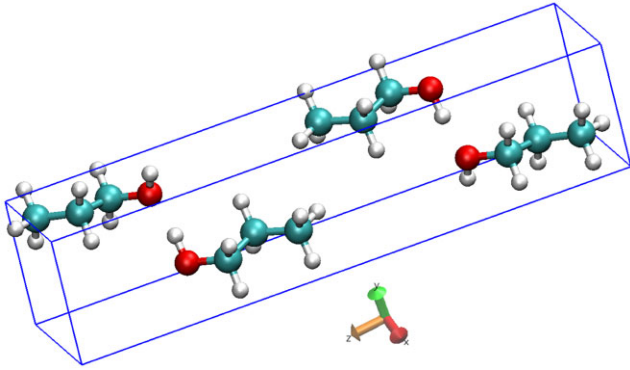


Figure 3. Predicted crystal structure for 1-propanol. Carbon, oxygen, and hydrogen atoms are shown in cyan, red, and white colour, respectively.

time-step of 1 fs. During the simulation, the Berendsen thermostat and barostat with a temperature coupling were used with a 1.0 ps time constant. As shown in Figure S8 (shown in the SI), the cell lengths level off quickly after a few hundred picoseconds at 10 K, which provides assurance that the crystal structure is stable enough to hold the configuration at this temperature. To obtain temperature-dependent behaviour, the post-equilibration configuration at 10 K was slowly heated to the required temperature, and then equilibrated for a few nanoseconds, following which it was heated to the next required temperature. The complete step-by-step temperature ramp is outlined in Figure S6 (in the SI).

3.2.2 Simulated IR spectra of 1-propanol and comparison

The simulated density of states of 1-propanol crystal structure in bulk phase was obtained for different temperatures through the course of annealing starting from 10 till 120 K. The spectra at the interval temperatures were computed for the range of 500–4000 cm^{-1} (please see Figure S9 in the SI). The spectrum of the simulated solid at 10 and 120 K was compared against the experimental IR spectrum at the same temperature, in Fig. 4. There is a good agreement between the calculations and experiments in the peak positions, except the peak corresponding to the OH stretching vibrations, which appears as a broad peak centred around 3400 cm^{-1} in the experiment, but in simulation, it appears as a shorter, sharper peak at $\sim 3700 \text{ cm}^{-1}$. The family of peaks in the 1100–850 cm^{-1} range that shows a uniform shift of $\sim 70 \text{ cm}^{-1}$ between simulated and experimental case correspond to the same vibrations: CH_3 rocking, $\text{CH}_3\text{-CH}_2$ stretching, and $\text{CH}_2\text{-O}$ stretching in both cases.

To interpret the experimentally observed behaviour of 1-propanol in relation to temperature from a molecular perspective, MD simulations were performed on a vacuum-deposited system of 400 1-propanol molecules on a KBr surface. To heat the system, a linear temperature ramp with a heating rate of 0.05 K/ps was employed. Following the deposition simulations and subsequent heating, the calculation of the DoS was carried out at various temperatures. The range of spectra for various temperatures is shown for the full range frequency range in Fig. 5. To identify the various trends in the spectra, it is convenient to zoom into the (1500–700 cm^{-1}) frequency region. In this region, many trends can be observed in the form of the appearance or disappearance of peaks, and the change in the relative heights of the peaks. As highlighted in Fig. 6, there are several peaks that show differences with respect to temperature in the 1500–700 cm^{-1} range.

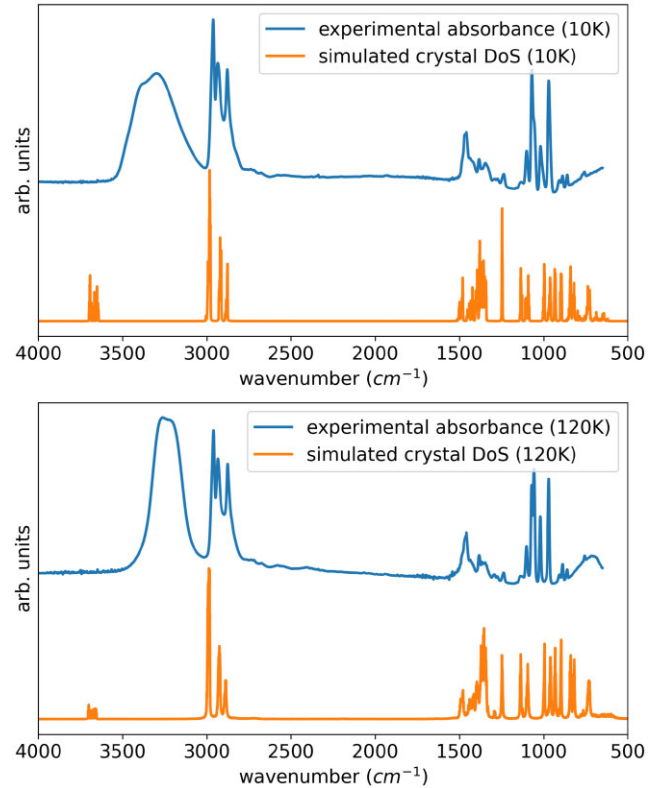


Figure 4. Comparison between the DoS of simulated bulk 1-propanol solid and experimentally obtained IR spectra of deposited 1-propanol at 10 K and 120 K.

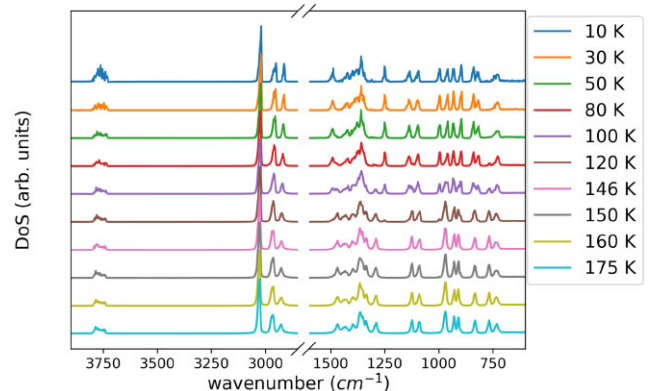


Figure 5. Simulated DoS spectra of the system of 400 molecules of 1-propanol deposited on the KBr substrate throughout a range of temperatures.

In Fig. 6, a number of spectral features have been highlighted to show the temperature variation of these respective peaks. Amongst these, the pair of peaks labelled ‘iv’ is worth paying attention to, as they are the peaks corresponding to the CH_3 rocking, $\text{CH}_2\text{-CH}_2$ stretching, and $\text{CH}_2\text{-O}$ stretching vibrations. They are located at $\nu_1 = 996 \text{ cm}^{-1}$ and $\nu_2 = 961 \text{ cm}^{-1}$. At 10 K, a lower wavelength peak is present and has a similar intensity to the higher wavelength peak. On heating, ν_1 begins to diminish in relative intensity while ν_2 gains intensity. At $T > 120 \text{ K}$, ν_1 has disappeared completely and ν_2 has a higher intensity than at 10 K. A concise description of the peaks and their temperature-dependent behaviours are listed as follows:

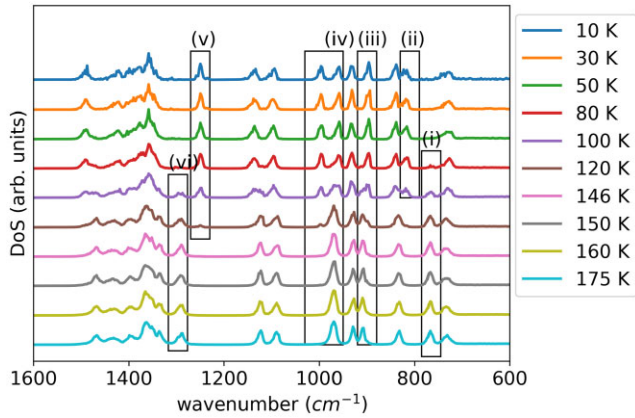


Figure 6. 1600–600 cm^{-1} range of the simulated IR spectra of the system of 400 molecules of 1-propanol deposited on the KBr substrate. Specific regions of interest have been marked and labelled.

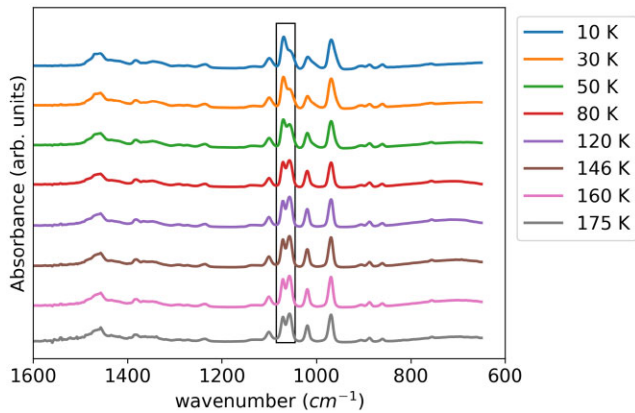


Figure 7. Experimental IR spectra zoomed in to 1600–600 cm^{-1} range. The highlighted pair of peaks at 1069 and 1059 cm^{-1} shows a trend of change in relative height that corresponds to a similar observation in the spectra of the simulated system.

- (i) Peak at 745 cm^{-1} is absent below 100 K but appears at 100 K and becomes prominent with increasing temperature.
- (ii) Peak at 820 cm^{-1} shows gradual disappearance with increasing temperature and is completely absent at $T > 120$ K.
- (iii) Peak at 900 cm^{-1} diminishes with increasing temperature and peak at 910 cm^{-1} becomes more prominent as temperature increases. Both peaks are visible at 100 and 120 K.
- (iv) Peak at 1000 cm^{-1} disappears with increasing temperature. Absent at 146 K and above.
- (v) Peak at 1250 cm^{-1} disappears with increasing temperature. Absent at 146 K and above.
- (vi) Peak at 1290 cm^{-1} absent below 100 K, and gains intensity with increasing temperature.

From the experimentally obtained IR spectra, shown in Figs 2 and 7, the highlighted pair of peaks at 1069 and 1059 cm^{-1} show a temperature-dependent behaviour which is similar to the pair of peaks labelled as ‘iv’ in Fig. 6. The lower wavelength peak shows decreasing intensity with heating in both scenarios, and the higher wavelength peak shows increasing intensity. The temperature where the overtaking happens is about 120 K in both cases. The effect is more pronounced in the case of simulation wherein the left-side peak is completely absent at lower temperatures; whereas in the

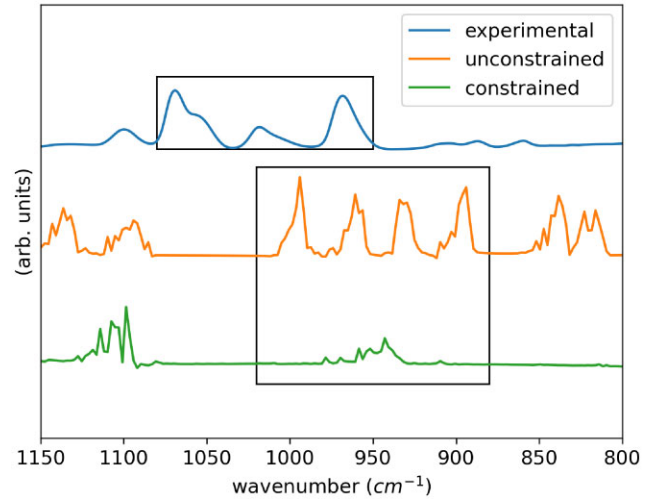


Figure 8. Comparison of the experimental IR spectra of 1-propanol, with the density of states obtained from MD simulation of the deposited 1-propanol system, as well as that of the deposited 1-propanol system after constraining the bond vibration of C–C and C–O to remove their contributions. The experimental IR as well as the simulated DoS were obtained at a temperature of 10 K.

experiment, said peak is visible but of lower intensity. With the similar behaviour observed between both cases and considering the ~ 70 cm^{-1} shift in the family of peaks as shown in Fig. 8, it can be stated that the two observations corroborate with each other.

By converting C–C and C–O bonds to constraints in the simulation topology, it is possible to single out peaks are contributions of the respective vibrations. In Fig. 8, it is seen that the peaks corresponding to CH_2 – CH_2 stretching, and CH_2 –O stretching have disappeared from the constrained simulation, with the only remaining contribution from CH_3 rocking. This further supports the claim that the family of peaks highlighted are the same vibrations, but with a uniform shift of ~ 70 cm^{-1} between the simulated and experimental observations.

At low temperatures, the thermal freedom available to the molecules in the deposited layer is low, and it increases as the temperature increases. This thermal freedom allows for the molecules to reorient themselves within the amorphous layer to achieve better close packing. This phenomenon is termed as ‘ice compaction’. Spectrally, this would manifest as the narrowing of peaks. In Fig. 9, the temperature-dependent trend in the width of the peak corresponding to the OH stretching vibration is observed. At 10 K, the peak starts off wide, and on heating, it becomes narrower until it reaches a minimum at around 120 K. On further heating, the peak begins to widen again until 175 K. The trend in this spectral feature is common across both the experimental and simulated spectra. The narrowing of the peaks is an indication of ice compaction, comparable to the observations of the breadth of the OH stretching band in the experimental data.

At the molecular scale, the driving factor behind the stability of a crystalline 1-propanol solid is the hydrogen-bonding network. Due to the presence of the hydroxyl (–OH) group in 1-propanol, there is a possibility of one hydrogen bond per molecule. The number of hydrogen bonds in the system was calculated for a range of temperatures and the average number of hydrogen bonds per molecule was plotted against temperature as shown in Fig. 10. In the predicted crystal structure obtained via CSP, the average number of hydrogen bonds per molecule remains fixed at 1, as the hydrogen bonding network is a driving factor in the stability of the crystal

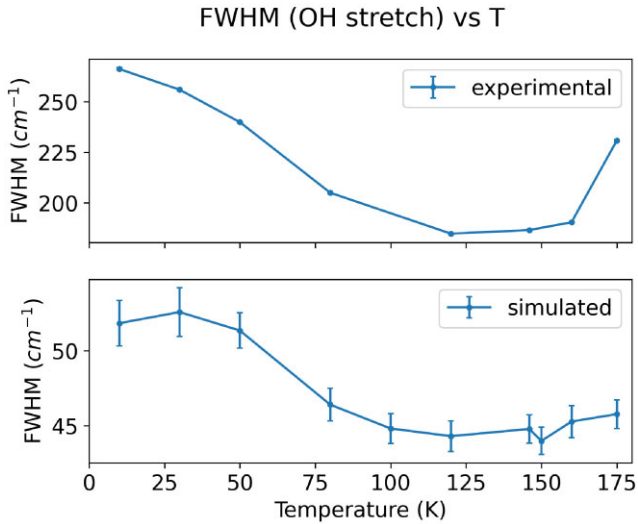


Figure 9. The O–H stretching bands in the experimental and simulated spectra fitted to a Gaussian profile, and their respective full width at half-maximum (FWHM) plotted against temperature. The error bars plotted are the standard error, defined as the square root of the corresponding diagonal element of the covariance matrix obtained during the fitting process.

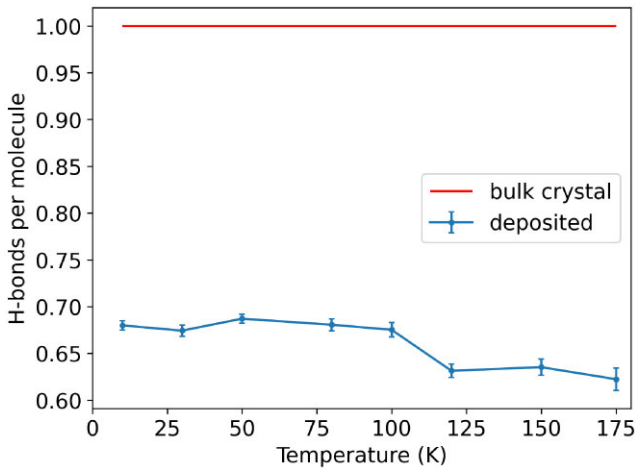
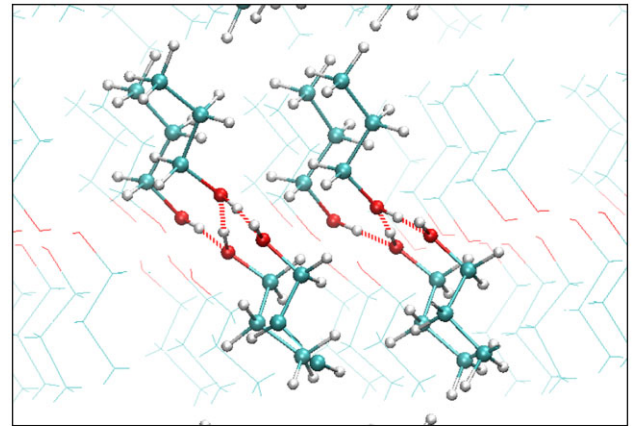
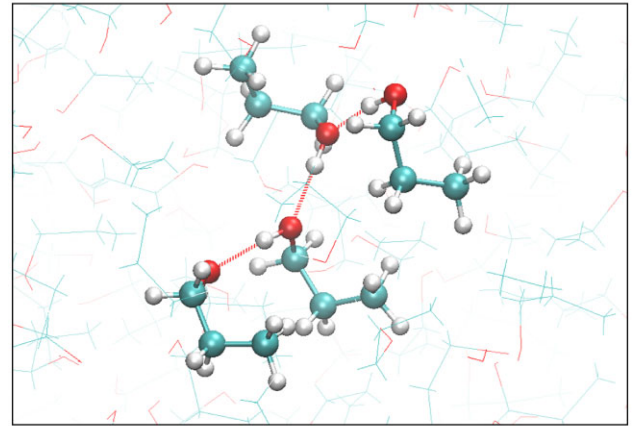


Figure 10. Number of hydrogen bonds per molecule in the simulated system for the range of temperatures. The calculation was done across a slice of 1 nm thickness parallel to the substrate. The average was done over 1000 configurations in the simulated trajectory. The bulk crystal data correspond to the predicted CSP structure. The hydrogen bond distance cut-off for calculation was 0.35 nm while the H–D–A angle cut-off was 30° .

structure. However, for the deposited system, which is amorphous in nature, the average number of hydrogen bonds per molecule is notably less than 1 for all temperatures. This highlights the tendency of the ice to not form a crystal as the hydrogen bonding network is not sufficient to facilitate the crystal structure, similar to what is observed experimentally. In Fig. 11, we show a visual comparison between the hydrogen-bonding network that is possible in the crystal arrangement versus the amorphous system. The possibility of every -OH group participating in a hydrogen bond is always satisfied in the crystal because of the orientational order; however, as we can predict and also observe from the computational results, this is not necessarily the case for the amorphous arrangement.



(a) Crystalline



(b) Amorphous

Figure 11. For the system of 1-propanol, the hydrogen bonding network is shown (a) in the crystal phase, and (b) in the amorphous phase. The dashed lines denote a hydrogen bond between a hydrogen atom and an oxygen atom.

4 CONCLUSION

With the discovery of 1-propanol in the ISM, it is necessary to characterize the physicochemical behaviour of the molecule at such conditions. Analysing the observational spectra strongly relies on laboratory-based data. Hence, in this paper, we presented the temperature-dependent IR spectra of 1-propanol ice, deposited at 10 K and then warmed to 170 K, revealed an amorphous morphology throughout the warming phase until sublimation. Although indications of ice compaction were observed, signatures specific to crystallization were absent. Knowing the phase of the molecule is especially important to calculate the accurate abundance of the molecule in the region of observation. Employing the tools of classical MD, we also conducted simulation studies of a vacuum-deposited 1-propanol ice system across the same temperature range as the experiment. From the simulations, we extracted various results including spectral and structural properties. The observed temperature-dependent trends across these results demonstrate a notable level of agreement between experiment and simulation, providing insights into the phase behaviour of the ice at a molecular scale. Most importantly, the key observation was the presence of 1-propanol on the substrate up to 170 K, despite the known melting point of 1-propanol being 147 K. It is worth noting that, to the best of our knowledge, this marks the first observation, or at least the first reporting, of a molecule staying on the substrate beyond its melting

point under such conditions. Based on the experimental and simulation results, we attribute this behaviour to the low vapour pressure of the molecule at such low temperatures, which we also confirmed through a series of experiments by maintaining the deposited ice at isothermal conditions at different temperatures beyond the melting point and below the sublimation temperature. Therefore, the reported results suggest that the morphology of the interstellar icy mantle containing 1-propanol, along with other molecules (particularly water), warrants further investigation, as the sublimation temperature of 1-propanol falls well within the range of crystallization and sublimation temperatures of several other molecules. Consequently, our future work will focus on the 1-propanol and water ice mixture.

ACKNOWLEDGEMENTS

PKM acknowledges funding through SERB, IRHPA (No. IPA/2020/000034) and BRNS(58/14/09/2021-BRNS/37116). RR, BNRS, AB, NJM, and BS thank NSRRC for providing beamtime for the measurements. RR, SG, JK, AB, and BS acknowledge the support from PRL (Dept of Space, Govt of India). AB acknowledges the J C Bose National Fellowship. BNRS, NJM, and BS acknowledge the support from Sir John and Lady Mason Academic Trust. NJM acknowledges support from the Europlanet-2024-RI. Europlanet 2024 RI has received funding from the European Union's Horizon 2020 research and innovation program under grant agreement no. 871149. We are grateful to Dr G. R. Desiraju of the Solid State and Structural Chemistry Unit, Indian Institute of Science for his assistance in connecting with Dr T. S. Thakur.

DATA AVAILABILITY

The data will be made available on request

REFERENCES

- Abplanalp M. J., Kaiser R. I., 2019, *Phys. Chem. Chem. Phys.*, 21, 16949
- Abraham M. J., Murtola T., Schulz R., P'all S., Smith J. C., Hess B., Lindahl E., 2015, *SoftwareX*, 1, 19
- Altwegg K. et al., 2017, *MNRAS*, 469, S130
- Ayling S. A., Burke D. J., Salter T. L., Brown W. A., 2017, *RSC Adv.*, 7, 51621
- Ball J. A., Gottlieb C. A., Lilley A., Radford H., 1970, *ApJ*, 162, L203
- Bussi G., Donadio D., Parrinello M., 2007, *J. Chem. Phys.*, 126
- Crovisier J., Bockelée-Morvan D., Biver N., Colom P., Despois D., Lis D. C., 2004, *A&A*, 418, L35
- Darden T., York D., Pedersen L., 1993, *J. Chem. Phys.*, 98, 10089
- Despois D., 1992, in Singh P. D., ed., Proc. IAU Symp. 150, Astrochemistry of Cosmic Phenomena. Kluwer, Dordrecht, p. 451
- Dodda L. S., Cabeza de Vaca I., Tirado-Rives J., Jorgensen W. L., 2017a, *Nucleic Acids Res.*, 45, W331
- Dodda L. S., Vilseck J. Z., Tirado-Rives J., Jorgensen W. L., 2017b, *J. Phys. Chem. B*, 121, 3864
- Doroshenko I., Pogorelov V., Sablinskas V., 2012, *Dataset Papers in Chemistry*, 2013, 329406
- Ehrenfreund P., Charnley S. B., 2000, *ARA&A*, 38, 427
- Essmann U., Perera L., Berkowitz M. L., Darden T., Lee H., Pedersen L. G., 1995, *J. Chem. Phys.*, 103, 8577
- Fuchs G., Cuppen H., Ioppolo S., Romanzin C., Bisschop S., Andersson S., Van Dishoeck E., Linnartz H., 2009, *A&A*, 505, 629
- Fuentes-Azcárral R., Barbosa M. C., 2018, *Physica A: Stat. Mech. Appl.*, 491, 480
- Hiraoka K., Mochizuki N., Wada A., 2006, AIP Conf. Proc. Vol. 855, Astrochemistry: From Laboratory Studies to Astronomical Observations. Am. Inst. Phys., New York, p. 86
- Hollis J. M., Jewell P. R., Lovas F. J., Remijan A., Møllendal H., 2004, *ApJ*, 610, L21
- Hudson R. L., Moore M. H., 2018, *ApJ*, 857, 89
- Jiménez-Serra I. et al., 2022, *A&A*, 663, A181
- Jorgensen W. L., Tirado-Rives J., 2005, *Proc. Natl. Acad. Sci.*, 102, 6665
- Kasamatsu T., Kaneko T., Saito T., Kobayashi K., 1997, *Bull. Chem. Soc. Japan*, 70, 1021
- Lin S.-T., Blanco M., Goddard W. A., 2003, *J. Chem. Phys.*, 119, 11792
- Lin S.-T., Maiti P. K., Goddard W. A. I., 2010, *J. Phys. Chem. B*, 114, 8191
- Lu H.-C., Chen H.-K., Cheng B.-M., Ogilvie J., 2008, *Spectrochim. Acta A*, 71, 1485
- Luna R., Molpeceres G., Ortigoso J., Satorre M. A., Domingo M., Maté B., 2018, *A&A*, 617, A116
- NIST, 2023, NIST Chemistry WebBook, SRD 69, <https://webbook.nist.gov/cgi/inchi/InChI>
- Nag S., Majumdar J., Sivaraman B., Yashonath S., Maiti P. K., 2023, *MNRAS*, 522, 3656
- Pavithra S. et al., 2017, *Spectrochim. Acta A*, 178, 166
- Pethes I., Pusztai L., Ohara K., Temleitner L., 2021, *J. Mol. Liq.*, 340, 117188
- Qasim D. et al., 2019, *A&A*, 627, A1
- Ramachandran R. et al., 2023, *J. Chem. Sci.*, 135, 77
- Ramírez-Cardona M., Ventolà L., Calvet T., Cuevas-Diarte M., Rius J., Amigó J., Reventós M., 2005, *Powder Diffr.*, 20, 311
- Ruiz-Mirazo K., Briones C., de la Escosura A., 2014, *Chem. Rev.*, 114, 285
- Stroet M., Sanderson S., Sanzogni A. V., Nada S., Lee T., Caron B., Mark A. E., Burn P. L., 2022, *J. Chem. Inf. Model.*, 63, 2
- Stromsoe E., Ronne H. G., Lydersen A. L., 1970, *J. Chem. Eng. Data*, 15, 286
- Tschamler H., Richter E., Wettig F., 1949, *Mon. hefte Chem. Verwandte Teile anderer Wiss.*, 80, 749
- Turner B. E., Apponi A. J., 2001, *ApJ*, 561, L207
- Watanabe N., Kouchi A., 2002, *ApJ*, 571, L173
- Yuan C., Smith R. S., Kay B. D., 2016, *Surf. Sci.*, 652, 350
- Zangi R., 2018, *ACS Omega*, 3, 18089
- Zuckerman B. et al., 1975, *ApJ*, 196, L99

SUPPORTING INFORMATION

Supplementary data are available at *MNRAS* online.

suppl_data

Please note: Oxford University Press is not responsible for the content or functionality of any supporting materials supplied by the authors. Any queries (other than missing material) should be directed to the corresponding author for the article.

This paper has been typeset from a $\text{\TeX}/\text{\LaTeX}$ file prepared by the author.